ADVANCED FUNCTIONAL MATERIALS
www.afm-journal.de

Two-Component Molecular Materials of 2,5-Diphenyloxazole Exhibiting Tunable Ultraviolet/Blue Polarized Emission, Pump-enhanced Luminescence, and Mechanochromic Response

Dongpeng Yan, Hejia Yang, Qingyun Meng, Heyang Lin, and Min Wei*

The development of π-conjugated molecular systems with high-efficiency generation of UV and blue light plays an important role in the fields of light-emitting diodes, fluorescent imaging, and information storage. Herein, supramolecular construction of solid-state UV/blue luminescent materials are assembled using 2,5-diphenyloxazole (DPO) with four typical co-assembled building blocks (1,4-diiodotetrafluorobenzene, 4-bromotetrafluorobenzene carboxylic acid, pentafluorophenol, and octafluoronaphthalene). Compared with the pristine DPO sample, the as-prepared two-component molecular materials feature ease of crystallization, high crystallinity, enhanced thermal stability and tunable luminescence properties (such as emissive wavelength, color, fluorescence lifetime, and photoluminescence quantum yield) as well as multicolor polarized emission in the UV/blue region. Moreover, pump-enhanced luminescence and reversible mechanochromic fluorescence (MCF) properties can also be obtained for these molecular solids, which are absent for the pristine DPO sample. Therefore, this work provides a procedure for the facile self-assembly of ordered two-component molecular materials with tunable UV/blue luminescence properties, which have potential application in the areas of light-emitting displays, polarized emission, frequency doubling, and luminescent sensors.

1. Introduction

Organic photoactive chromophores have recently received increasing attention due to their unique optical properties and promising optoelectronic applications in the fields of lasers,[1] waveguides,[2] sensors,[3] and polarized luminescence.[4] Compared with their inorganic counterpart, organic photofunctional materials generally offer the advantages of simple processing and easily tunable structure, which facilitates the fabrication of flexible and soft optical device.[5] However, key scientific and technologic problems, such as their relatively poor thermal/optical stability and low crystallinity—particularly for low-molecule-weight compounds[6]—must be resolved before these photoactive molecules can be employed in practical optoelectronic devices. Moreover, setting up effective ways to tune and control the photophysical properties of an organic material is a prerequisite for developing new generation multiple-color luminescent devices.[7] It is well known that the intermolecular interactions and molecular orientation/arrangement in the solid-state materials can strongly influence the bulk properties.[8] For example, non-centrosymmetric photoactive molecular solids afford the possibility of second harmonic generation (SHG) for nonlinear optics applications.[9] However, up to now, efforts to obtain functional materials with desirable photophysical properties through rational tailoring the environment of the photoactive molecules within a molecular solid remain at an early stage.[10] In addition, compared with the development of green/red light-emitting materials, the high efficiency generation of UV and blue light in molecular systems continues to be a challenge,[10] although UV/blue luminescence has great potential uses in light-emitting diodes for full-color display,[11] fluorescent imaging of cells,[12] and information storage device.[13]

Recent advancements in supramolecular materials have allowed the assembly of multi-component molecular solids (such as cocrystals and salts) based on the molecular recognition between the photoactive molecules and co-assembled building blocks (coformers).[14] In these multi-component crystalline solids, the crystal packing and structure can be modified by rational selection and design of the intermolecular interactions (such as halogen/hydrogen bonds and π–π interaction), and thus the desirable solid-state properties—such as tunable fluorescence and light-induced patterning efficiency—can be achieved.[15] Importantly, the relative weak supramolecular interactions between the components in a molecular solid can be further tailored by external perturbations (such as grinding and mechanical stimuli), which results in the ability to control and switch the bulk luminescent properties.[16] Such a strategy may pave a new way for developing stimuli-responsive photofunctional materials,

Dr. D. Yan, H. Yang, Prof. Q. Meng,
H. Lin, Prof. M. Wei
State Key Laboratory of Chemical
Resource Engineering
Beijing University of Chemical Technology
Beijing, 100029, PR China
E-mail: yandp@mail.buct.edu.cn

DOI: 10.1002/adfm.201302072

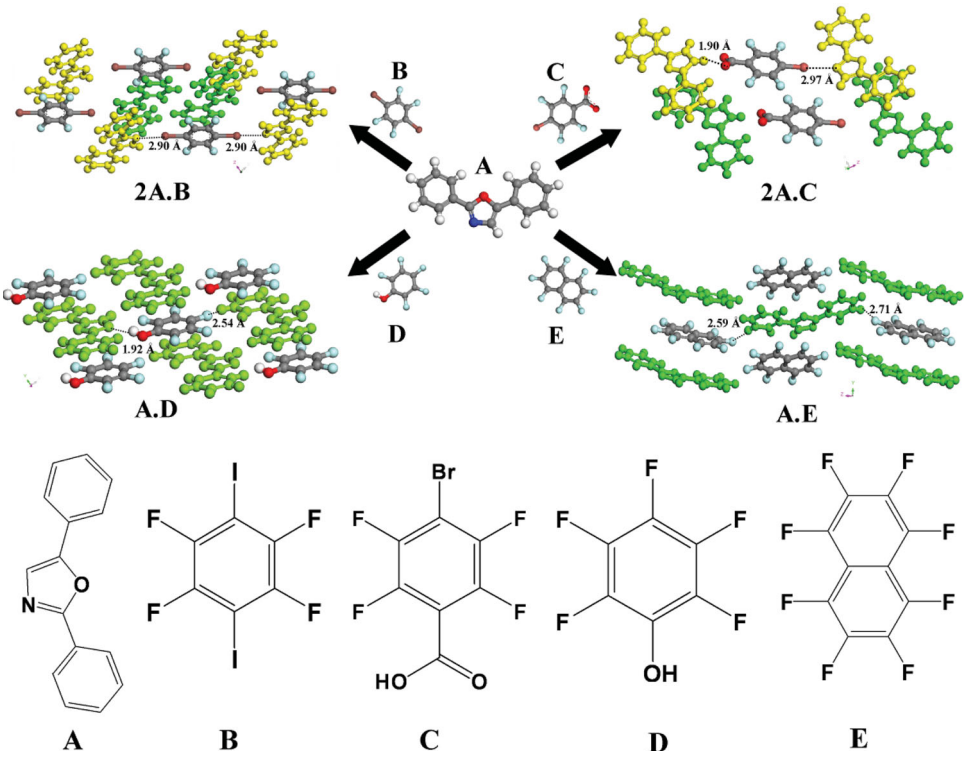

Scheme 1. (A) 2,5-Diphenyloxazole, (B) 1,4-diiodotetrafluorobenzene, (C) 4-bromotetrafluorobenzene carboxylic acid, (D) pentafluorophenol, (E) octafluoronaphthalene.

although examples of such multi-component molecular materials in this field are still rather rare.[16b]

2,5-Diphenyloxazole (DPO, **A**) is a well-known UV fluorescent molecule,[17] which is commonly used as a scintillator and liquid laser dye[18] due to its high photoluminescence quantum yield (PLQY) and intriguing luminescent properties. However, the crystallinity and melting point of solid DPO are relative low and high quality single crystal cannot be obtained, which restricts its further applications into solid-state photofunctional materials. Herein, based on the expectation of change in the crystal structures and stacking of fluorescent molecules for potential UV/blue light-emitting application, new DPO-based two-component single crystals have been synthesized by selecting coformers with different potential halogen or hydrogen bonding interaction modes with the N atom in the oxazole group of DPO as well as the possibility of π–π interactions between the assembled units. We describe how enhanced thermal stability and new photophysical properties (such as polarized UV/blue emission, second-order optical nonlinearity and mechanochromic fluorescence) can be endowed and varied within the multi-component organic solids relative to the pure DPO compound.

2. Results and Discussion

2.1. Structural Study on Two-Component Molecular Solids

Four representative fluorine-containing compounds (**B**–**E**, **Scheme 1**) lacking visible solid-state fluorescence were chosen as the coformers for **A**. In contrast to the low crystalline quality of pure DPO, the DPO-based two-component single crystals (**2A.B**, **2A.C**, **A.D**, **A.E**) can be readily formed by the slow evaporation of a methanol solution containing **A** and the appropriate coformers with a 2:1 stoichiometry for **2A.B**, **2A.C** and 1:1 for **A.D** and **A.E**. Single-crystal X-ray diffraction measurements (CCDC: 926585–926588) show that the **2A.B**, **2A.C** and **A.D** crystalline solids are assembled via the expected halogen and/or hydrogen bonding between the oxazole group in **A** and the halogen/carboxylic acid/hydroxyl units in the coformers. Upon assembly of **A** with coformer **B** to obtain cocrystal **2A.B**, the **A** molecules are ordered via N···I halogen bonds (distance: 2.90 Å) between the iodine in coformer **B** and the nitrogen in **A**, and the neighboring **A** molecule are arranged antisymmetrically and parallel with each other. For **2A.C**, the assembly fashion is similar to cocrystal **2A.B** with the **A** molecules parallel with each other (interplanar distance: 3.57 Å) and orientation angle between adjacent **A** of 43.7°, favoring the formation of J-type aggregates; the **A** molecules and coformer **C** are assembled via both N···Br halogen (distance: 2.97 Å) and COOH···N hydrogen bonding (distance: 1.90 Å). Within the crystal structure, proton transfer has taken place from the carboxylic acid group to the oxazole nitrogen atom, resulting in the formation of a salt. In addition, both **A** and **C** exhibit orientational disorder within the crystalline solid, and this may be assigned to the similar interaction strengths of halogen and hydrogen bonding within the crystal. For **A.D**, two hydrogen bonds—one N···H–O (distance: 1.92 Å) and one F···H–C (distance: 2.54 Å)—are formed between the **A** molecule and coformer **D**. For **A.E**, **A** molecules are disordered due to the low rotational energy barrier, and thus

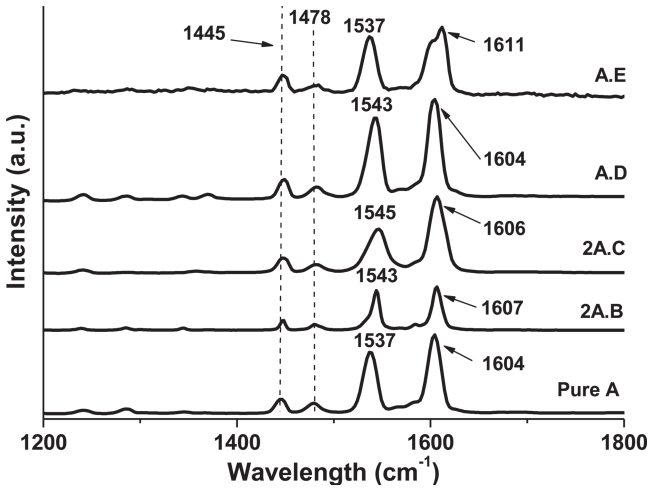

Figure 1. Raman spectra for pure **A**, **2A.B**, **2A.C**, **A.D** and **A.E**.

disordered packing occurs during the cocrystallization. **A** and **E** molecules are assembled by two F···H–C hydrogen bonds (distance: 2.59 and 2.71 Å). Both **A.D** and **A.E** present a layered structure with **A** and its coformers arranged alternately within the crystal (Scheme 1), where molecules within adjacent layer are mainly organized through π–π interactions. More detailed crystal information[19] is tabulated in Table S1 in Supporting Information.

Thermogravimetric–differential thermal analysis (TG-DTA) measurements (Figure S1 in Supporting Information) show that the melting points of the two-component molecular solids occur at higher temperatures (101–107 °C) than the pure **A** (79 °C), confirming that the thermal stability of the DPO can be improved by formation of multi-component solids. Moreover, Raman spectroscopy was employed to characterize the molecular vibrations within the pure **A** and the DPO-based two-component solids due to the highly symmetric structure of DPO (**Figure 1**). For the pristine **A**, the characteristic C=C stretching vibration bands of phenyl group appear at 1445, 1478, and 1604 cm^{-1}, and the peak located at 1537 cm^{-1} can be assigned to the C=N vibration of oxazole group. Upon assembly with the coformer **B**, **C**, and **D**, only slight change appeared in the C=C vibration bands at 1604 cm^{-1} towards 1607 and 1606 cm^{-1} for **2A.B** and **2A.C**, while the C=N vibration bands experienced an obvious high-frequency shift and were located at 1543 cm^{-1} (Δ = 6 cm^{-1}), 1545 (Δ = 8 cm^{-1}) and 1543 cm^{-1} (Δ = 6 cm^{-1}) for **2A.B**, **2A.C** and **A.D** respectively, indicative of the relative strong halogen and hydrogen bonding interaction between the coformer and N atoms in the oxazole group. For **A.E**, the C = C vibration bands underwent a blue-shift to 1611 cm^{-1} (Δ = 7 cm^{-1}), indicating that the **E** molecules can polarize and delocalize the electronic density of the **A** molecules within adjacent layer, which weakens the C = C bond in DPO to some extent. In addition, there was no shift in the C=N vibration compared with the that for pure **A**, which is consistent with the crystal structure which shows that there is no direct interaction between **E** and the oxazole group in **A**.

2. 2. Tunable Fluorescence and Polarized Emission

The four as-obtained two-component crystals exhibited different fluorescent behaviors from that of the pristine **A**, and the resulting excitation and emission spectra are shown in **Figure 2**a and b. Pure **A** has a maximum emission (λ_{em}^{max}) at 392 nm (S_1–S_0 transition) and two shoulder peaks at 377 and 412 nm, corresponding to 0–0 and 0–2 vibronic transition, respectively.[17] There is no obvious shift of λ_{em}^{max} for **2A.B** and **A.E**, but the shoulder peak at 377 nm is no longer observed. Cocrystal **A.D**, however, shows a marked blue shift with λ_{em}^{max} at 383 nm and a shoulder peak at 400 nm, which may be attributed to the disaggregation of the DPO induced by the blocking effect of **E**; whilst salt **2A.C** features

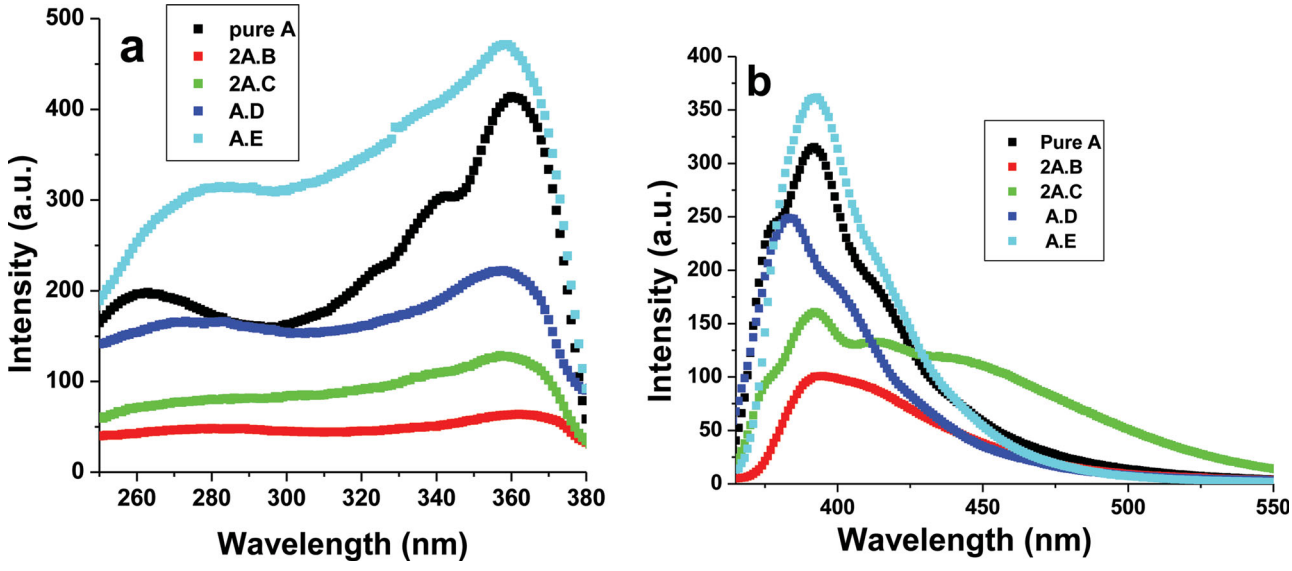

Figure 2. Excitation (a) and emission (b) spectra for **A**, **2A.B**, **2A.C**, **A.D** and **A.E**.

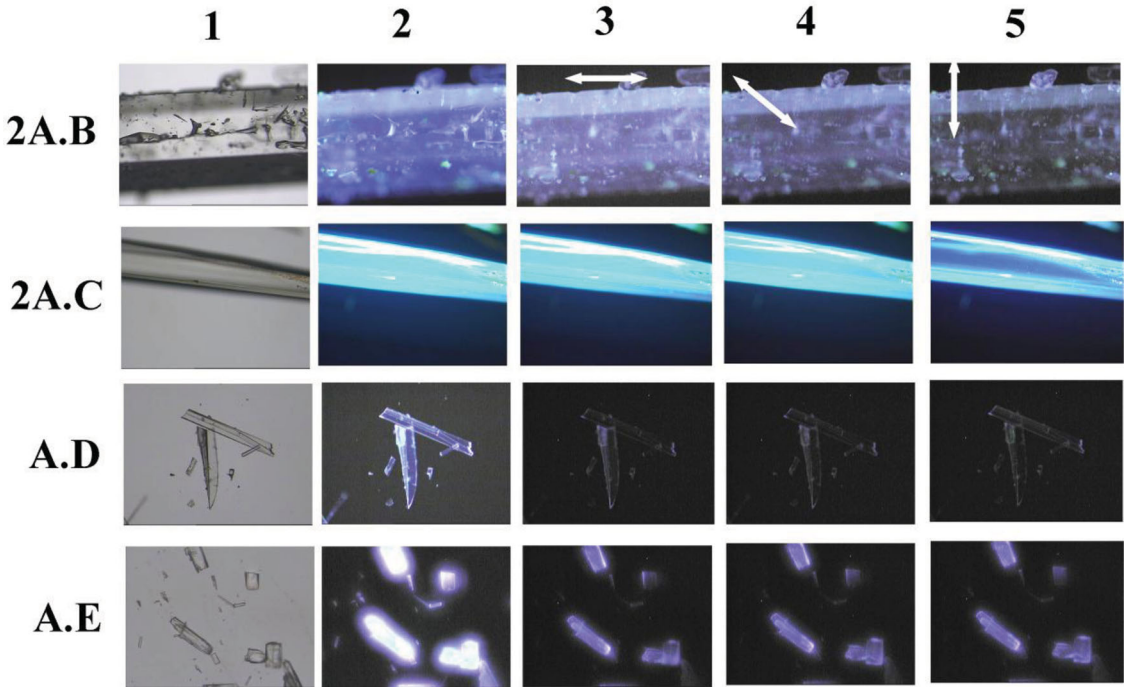

Figure 3. Photographs of solid-state multi-component crystals (**2A.B**, **2A.C**, **A.D** and **A.E**) multiplied by 50-fold: 1),2): the single crystals under daylight and UV (360 nm); 3),4),5): the samples under a polarized UV fluorescence microscope with the polarized directions of 0°, 45° and 90°.

a completely new broad peak at ca. 450 nm giving color coordinates of (0.149, 0.104) compared with those of the pure **A** ((0.159, 0.039)). Such behavior is consistent with the formation of J-type aggregates between the adjacent **A** molecules within the salt. Additionally, the two-component molecular materials also exhibit variable PLQY in the range from 3.9% (**2A.B**) to 55.6% (**A.E**), illustrating that the PLQY values can be tuned over a wide range compared with the value for the pristine **A** sample (45.7%). To obtain an insight into the excited states responsible for fluorescence of these solids, the fluorescence lifetimes were measured and the corresponding fluorescence decay curves are shown in Figure S2 in Supporting Information. The fluorescence lifetimes of **2A.B**, **2A.C**, **A.D** are in the range 0.21–0.29 ns (Supporting Information: Table S2), whereas for **A.E** the value is 1. 82 ns, slightly larger than the value for the pure **A** (1.45 ns). The fluorescence lifetime results are consistent with the trend of PLQY. Specifically, the enhanced PLQY and fluorescence lifetime for **A.E** may be attributed to **E** molecules isolating the interaction between DPO chromophores, and thus suppressing aggregation in the solid state.

Luminescent color coordinate results confirm that the fluorescence of these samples is mainly populated in the UV/blue region (Table S2 in Supporting Information). Under a fluorescence microscope, the well-defined photoemission (**Figure 3**.2) of the transparent two-component crystals (Figure 3.1) can be easy imaged. When the single crystals was excited with the excitation light polarized parallel to their long-axis direction, the emission intensities varied obviously between the parallel (I) and perpendicular (I) polarized directions, as observed in Figure 3.3, 3.4, and 3.5 for the polarized directions 0°, 45°, and 90°, respectively. Polarized fluorescence measurements were further employed to probe the fluorescence anisotropic value r.[20] Typical polarized fluorescence profiles for the individual single crystals are shown in **Figure 4**a–d. The anisotropic values (r) for the four two-component crystals are in the range of 0.32–0.42 at the λ_{em}^{max}. Taking **2A.B** as an example, the crystals shows UV fluorescence anisotropy between the directions parallel and perpendicular to excitation polarized direction (I_{VV} *vs.* I_{VH}) with the r value of ca. 0.42, slightly larger than the highest value of 0.4 for a system without macroscopic alignment.[21] The polarized anisotropy is related to the highly ordered arrangement of the DPO molecules within the two-component crystals. Therefore, it can be concluded that the new DPO-based multi-component molecular materials exhibit tunable UV/blue polarized fluorescence.

2.3. Two-Photon-Excited Fluorescence and Pump-Enhanced Luminescence

To detect any two-photon-excited UV/blue fluorescence of the multi-component molecular solids, long-wavelength-excited fluorescence measurements were thus further made. Upon excitation by 800 nm laser light, pure **A** sample exhibited low-wavelength fluorescence with an asymmetrical emission peak at 396 and a shoulder one at 412 nm (**Figure 5**a), close to the emission bands obtained by excitation with 360 nm UV light above. The emission intensity has a linear dependence on the incident energy square, illustrating that the emission process involves two-photon excited states to the ground state. For **2A.B**, weak pump-enhanced luminescence at ca. 400 nm can be observed

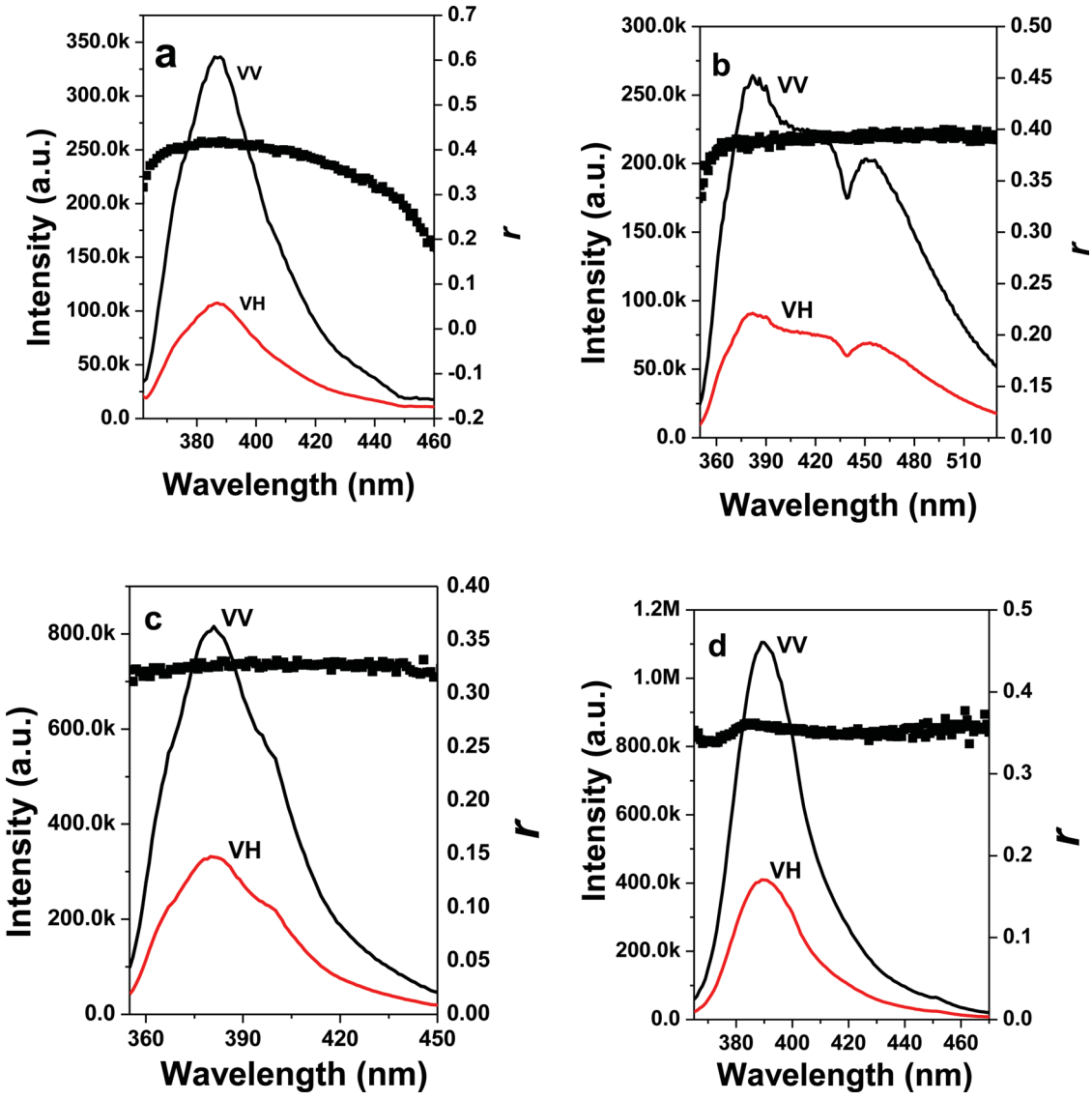

Figure 4. Polarized fluorescence profiles in the VV, VH modes and anisotropic values for the individual crystals of a) **2A.B**, b) **2A.C**, c) **A.D** and d) **A.E**.

(Figure S3a in Supporting Information), which can be assigned to the second harmonic generation (SHG) effect. The low intensity is probably due to the centrosymmetry and low PLQY of the **2A.B**; while the **2A.C** (Figure 5b) exhibits strong emission at 400 nm, and the emission intensity shows a nearly quadratic increase as a function of the incident energy as shown in the inset of Figure 5b, confirming the second-order optical nonlinearity. The strong SHG for **2A.C** can be related to the disordered arrangements of the **A** and **C** molecules, which reduce the symmetry of the chromophore within the molecular solid. Similar SHG behavior with pump-enhanced luminescence output was also observed for non-centrosymmetric **A.D** (Figure S4b in Supporting Information). In addition, considering the DPO component is also within the **2A.C** and **A.D** crystal, the absence of the broad two-photon emission band in the **2A.C** and **A.D** may be attributed to the fact that the **2A.C** and **A.D** has much lower PLQY (7.4% and 3.4%) than the pure DPO sample (45.8%), since the low PLQY value can largely restrict the efficiency of the two-photon absorption/emission and the detection of the spectra. For the non-centrosymmetric **A.E** sample (Figure 5c), besides the sharp laser peak at 400 nm, UV/blue emission in the range 370–475 nm can also be observed, suggesting that a combination of SHG and two-photon-excited fluorescence occurs due to the very high PLQY of **A.E**. Therefore, it can be concluded that the transformation from two-photon-excited fluorescence to SHG effect can be achieved by the assembly of pristine DPO within the two-component crystals with disordered orientations and/or non-centrosymmetric structures.

2.4. Mechanochromic Fluorescence

The two-component molecular solids **2A.B**, **2A.C**, and **A.D** also displayed change in fluorescence properties when the crystals

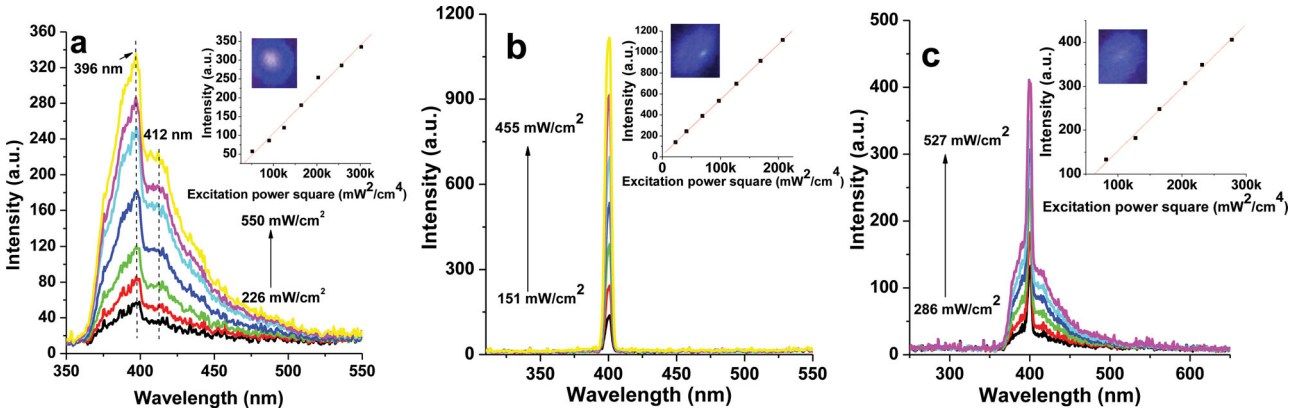

Figure 5. Fluorescence spectra of the pure **A** (a) and cocrystal **2A.C** (b) and **A.E** (c) excited by 800 nm laser under different pump powers. Insets show the changes in intensity at 400 nm with increasing pump power square and photographs of samples under 800 nm laser.

were ground into powder form. For **2A.B**, the photoemission band moved from 393 nm to 384 nm accompanied by the appearance of the shoulder peak at 374 nm and a slight increase in the luminescence intensity (**Figure 6**a). Similar phenomena can also be observed for **A.D**, with a new shoulder peak occurring at 365 nm (Figure 6c). In contrast, **2A.C** showed a completely different emissive spectrum with the dominating band at 449 nm and a shoulder peak at 373 nm upon grinding (Figure 6b). The changes of their emission can also be visible (insets of Figure 6a–c). There was no obvious change in the emissive spectra for **A.E** and pristine **A** samples after application of pressure (Figure 6d and Figure S4 in Supporting Information). To better understand the interesting luminescent mechanochromism, powder X-ray diffraction (XRD) measurements were performed on the two-component solids before and after grinding. It was observed that the (020) and (002) diffraction peaks of **2A.B** and **A.D** underwent a shift towards high-angle (Figure S5a, S5c in Supporting Information), indicative of a decrease in the basal spacing in the (*0l0*) and (*00l*) directions (Figure S6 in Supporting Information) upon compression. The contraction in lattice distance can induce strong π–π interactions, leading to the increased aggregation of the DPO chromophores, and thus influence the luminescent properties. Moreover, for **2A.B**, the absence of several diffraction peaks (such as (011) and (111) peaks) suggests the appearance of amorphous phases upon grinding, since it has been demonstrated that the formation of amorphous states can also lead to the change in fluorescence.[22] For **2A.C** (Figure S5b in Supporting Information), in addition to the shift of the (002) peak to high degree, a new peak at 12.4° also appears upon grinding, indicating the formation of a new polymorph phase of **2A.C**, consistent with the substantial shift in the emission to longer wavelength. Additionally, there was no obvious change in the XRD pattern of **A.E** after grinding, except for a decrease in the peak intensities (Figure S5d in Supporting Information). The reversibility of the luminescence for **2A.B**, **2A.C** and **A.D** were further studied. When the ground **2A.B** and **A.D** powders were exposed under chloroform solvent, their fluorescence emission bands (Figure 6a,c) can partially return its original color together with the associated reverse spectral changes. When treating the ground **2A.C** sample, the emissive spectra have no significant change except for the disappearance of the shoulder band at 373 nm, whereas the fluorescence can be nearly recovered after recrystallization from methanol (Figure 6b). The reversible nature of mechanochromic fluorescence (MCF) properties likely arises from the recoverable intermolecular interactions, relative orientation and distance between the DPO and its coformers. To the best of our knowledge, although MCF has been reported for pure organic compounds,[23] liquid crystals,[24] metal-organic complexes[25] and polymer systems,[26] there have been very few examples of multi-component molecular solid systems exhibiting MCF. The formation of multi-component crystals may supply an alternative strategy for developing new MCF systems.

3. Conclusion

Supramolecular two-component crystalline materials containing 2,5-diphenyloxazole (DPO) have been fabricated based on halogen/hydrogen bonds and π–π interaction. The resulting DPO-based solids exhibit ease of crystallization, high crystallinity, enhanced thermal stability and tunable luminescence properties (such as emissive wavelength, color, fluorescence lifetime, and PLQY) as well as multi-color polarized emission in the UV/blue region. Interestingly, SHG and MCF properties can also be obtained for these crystalline samples. The pristine DPO shows no SHG and MCF behavior at all and the transformation of an SHG-free and MCF-free organic fluorophore into SHG and MCF materials by the formation of multi-component solids is the most distinctive feature of this work. The new properties make PDO-based molecular materials potential candidates for solid-state UV/blue opto-electronic applications, including polarized emission, frequency doubling, mechanochromic luminescent sensors, and fluorescent anti-forgery devices. It is also anticipated that the design and assembly principles of multi-component solids with tunable molecular orientation and packing mode, crystal symmetry and intermolecular fashion can be utilized to develop other new types of crystalline molecular materials for SHG and luminescent sensor application.

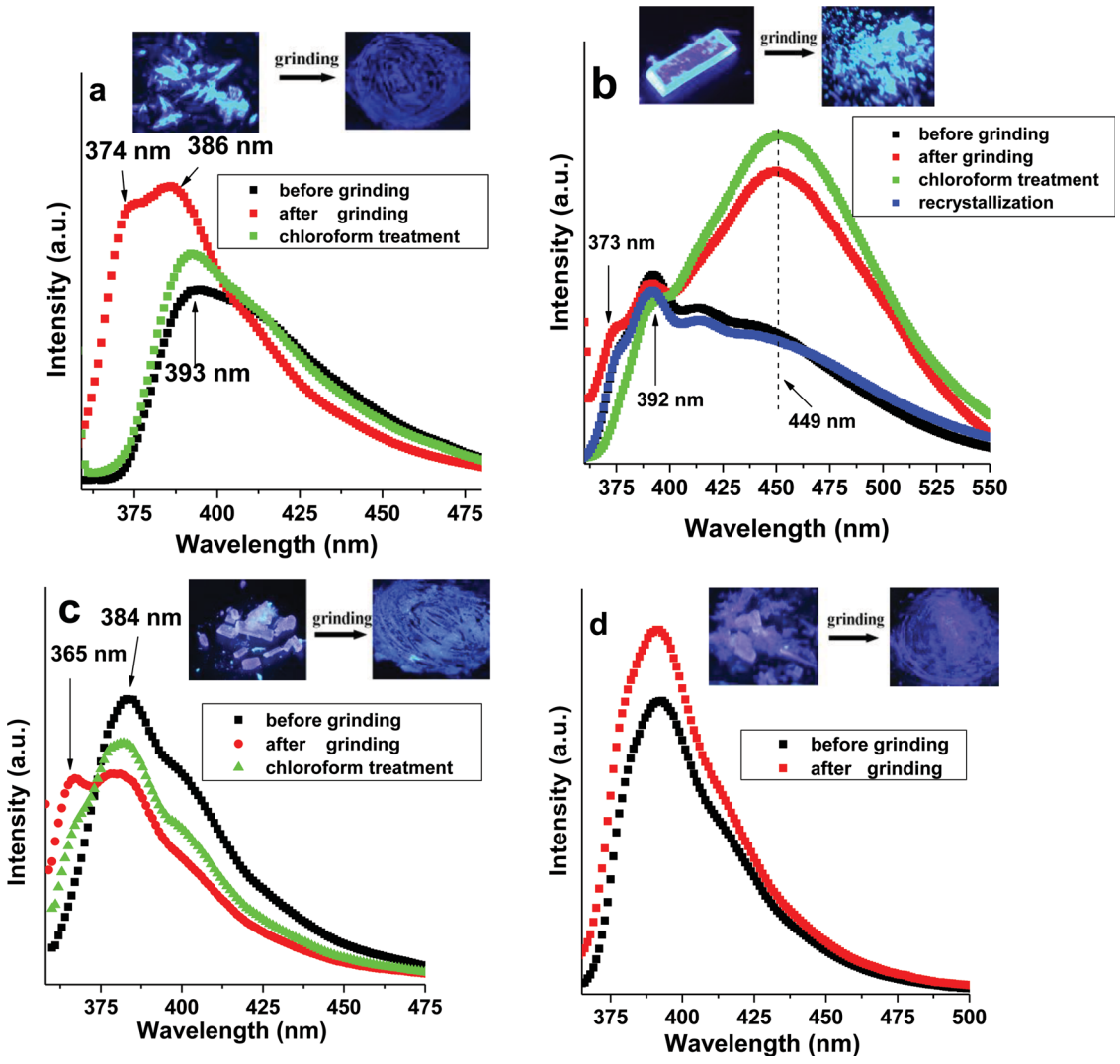

Figure 6. Fluorescence spectra of the a) **2A.B**, b) **2A.C**, c) **A.D** and d) **A.E**. before and after grinding. The spectra of ground powders treated with chloroform in a–c) and after recrystallization in b) are also shown. Insets show photographs of samples under UV light before and after grinding.

4. Experimental Section

Reagents and Materials: 2,5-Diphenyloxazole (**A,** DPO), 1,4-diiodotetrafluorobenzene (**B**), 4-bromotetrafluorobenzene carboxylic acid (**C**); pentafluorophenol (**D**); octafluoronaphthalene (**E**) were purchased from Sigma Chemical. Co. Ltd. and used without further purification.

Preparation of the DPO-based Crystal Systems: In typical reactions, the DPO-based two-component crystals (**2A.B**, **2A.C**, **A.D** and **A.E**.) can be obtained by slow evaporation of a methanol or chloroform solution (100 mL) containing 0.1 g solid mixtures of **A** and its coformer compounds with 2: 1 (**B** and **C**) or 1:1 (**D** and **E**) ratio, respectively. Single crystals were formed within two weeks.

Characterization: Single crystal X-ray diffraction data for DPO-based crystals **2A.B**, **2A.C**, **A.D** and **A.E**. were collected on a Nonius Kappa CCD diffractometer equipped with a graphite monochromator and an Oxford cryostream, using Mo$K\alpha$ radiation. Powder X-ray diffraction patterns (XRD) were recorded using a Rigaku 2500VB2+PC diffractometer under the following conditions: 40 kV, 50 mA, Cu Kα radiation (λ = 0.154056 nm) with step-scanning in steps of 0.04° (2θ) in the range from 4 to 25° using a count time of 10 s/step. TG-DTA was measured on a PCT-1A thermal analysis system under ambient atmosphere with a heating rate of 10 °C/min. The fluorescence spectra were recorded on a Shimadzu RF-5301PC spectrofluorimeter with the excitation source of 360 nm illuminating the solid-state sample at an incidence angle of 45°. Both the excitation and emission slits were set to be 3 nm. Steady-state polarized photoluminescence measurements were carried out with an Edinburgh Instruments FLS 920 spectrofluorimeter. The fluorescence decays were measured using an LifeSpec-ps spectrometer, and the lifetimes were calculated with the F900 Edinburgh instruments software. Photoluminescence quantum yield (PLQY) and 1931 CIE color coordinates were measured using an HORIBA Jobin-Yvon FluoroMax-4 spectrofluorimeter, equipped with an F-3018 integrating sphere. Two-photon-excited fluorescence of the samples was excited by 800 nm laser on a Tsunami-Spitfire-OPA-800C ultrafast optical parameter amplifier (Spectra Physics). The fluorescence images were obtained on an Olympus U-RFLT50 fluorescence microscope.

Supporting Information

Supporting Information is available from the Wiley Online Library or from the author. It includes single crystal structures for **2A.B**, **2A.C**, **A.D**

and **A.E** (Table S1); TG-DTA curves for pure **A**, **2A.B**, **2A.C**, **A.D** and **A.E** (Figure S1); PLQY, CIE 1931 color coordinates, and fluorescence lifetime of the two-component samples and **A** (Table S2); Fluorescence decay curves of the DPO-based molecular solids (Figure S2); Fluorescence spectra of **2A.B** and **A.D** excited by 800 nm laser under different pumping intensities (Figure S3); Fluorescence spectra of the pure **A** before and after grinding (Figure S4); XRD patterns for **2A.B**, **2A.C**, **A.D** and **A.E** before and after grinding treatment and the simulated XRD patterns (Figure S5); **2A.B**, **2A.C** and **A.D** viewed from (*0l0*) and (*00l*) directions (Figure S6).

Acknowledgements

This work was supported by the National Basic Research Program of China (Grant No.: 2014CB932103), the National Natural Science Foundation of China, the 111 Project (Grant No.: B07004), Central University Research Funds, and Program for Changjiang Scholars and the Innovative Research Team in University (PCSIRT: IRT1205).

Received: June 17, 2013
Revised: July 10, 2013
Published online: August 28, 2013

[1] a) R. H. Friend, R. W. Gymer, A. B. Holmes, J. H. Burroughes, R. N. Marks, *Nature* **1999**, *397*, 121; b) S. Tu, S. H. Kim, J. Joseph, D. A. Modarelli, J. R. Parquette, *J. Am. Chem. Soc.* **2011**, *133*, 19125.

[2] a) H. Yanagi, T. Ohara, T. Morikawa, *Adv. Mater.* **2001**, *13*, 1452; b) D. O'Carroll, I. Lieberwirth, G. Redmond, *Nat. Nanotechnol.* **2007**, *2*, 180; c) Y. Zhao, H. B. Fu, A. D. Peng, Y. Ma, D. B. Xiao, J. N. Yao, *Adv. Mater.* **2008**, *20*, 2859; d) C. Shi, Z. Guo, Y. Yan, S. Zhu, Y. Xie, Y. S. Zhao, W. Zhu, H. Tian. *ACS Appl. Mater. Interfaces* **2013**, *5*, 192.

[3] a) Y. Che, L. Zang, *Chem. Commun.* **2009**, 5106; b) Z. Ning, Z. Chen, Q. Zhang, Y. Yan, S. Qian, Y. Cao, H. Tian, *Adv. Funct. Mater.* **2007**, *17*, 3799; c) Y. Sagara, T. Kato, *Nat. Chem.* **2009**, *1*, 605; d) D. Yan, J. Lu, J. Ma, S. Qin, M. Wei, D. G. Evans, X. Duan, *Angew. Chem. Int. Ed.* **2011**, *50*, 7037; e) D. Yan, J. Lu, J. Ma, M. Wei, D. G. Evans, X. Duan, *Angew. Chem. Int. Ed.* **2011**, *50*, 720.

[4] a) K. Balakrishnan, A. Datar, R. Oitker, H. Chen, J. Zuo, L. Zang, *J. Am. Chem. Soc.* **2005**, *127*, 10496; b) F. Gao, Q. Liao, Z. Xu, Y. Yue, Q. Wang, H. Zhang, H. Fu, *Angew. Chem. Int. Ed.* **2010**, *49*, 732; c) D. Yan, W. Jones, G. Fan, M. Wei, D. G. Evans, *J. Mater. Chem. C* **2013**, *1*, 4138.

[5] A. Vidyasagar, K. Handore, K. M. Sureshan, *Angew. Chem. Int. Ed.* **2011**, *50*, 8021.

[6] H. Zhang, B. Yang, Y. Zheng, G. Yang, L. Ye, Y. Ma, X. Chen, G. Cheng, S. Liu, *J. Phys. Chem. B* **2004**, *108*, 9571.

[7] a) D. Yan, A. Delori, G. O. Lloyd, T. Friščić, G. M. Day, W. Jones, J. Lu, M. Wei, D. G. Evans, X. Duan, *Angew. Chem. Int. Ed.* **2011**, *50*, 12483; b) D. J. Wuest, *Nat. Chem.* **2012**, *4*, 74; c) D. Yan, A. Delori, G. O. Lloyd, B. Patel, T. Friščić, G. M. Day, D. K. Bučar, W. Jones, J. Lu, M. Wei, D. G. Evans, X. Duan, *CrystEngComm* **2012**, *14*, 5121; d) D. Yan, D. K. Bučar, A. Delori, B. Patel, G. O. Lloyd, W. Jones, X. Duan, *Chem. Eur. J.* **2013**, *19*, 8213; e) D. Yan, B. Patel, A. Delori, W. Jones, X. Duan, *Cryst. Growth Des.* **2013**, *13*, 333; f) D. Yan, D. G. Evans, *Mater. Horiz.* 2013, DOI:10.1039/C3MH00023K.

[8] a) T. Mutai, H. Satou, K. Araki, *Nat. Mater.* **2005**, *4*, 685; b) Y. Zhao, H. Gao, Y. Fan, T. Zhou, Z. Su, Y. Liu, Y. Wang, *Adv. Mater.* **2009**, *21*, 3165; c) Z. Zhang, B. Xu, J. Su, L. Shen, Y. Xie, H. Tian, *Angew. Chem. Int. Ed.* **2011**, *50*, 11654; d) S. Hirata, K. Totani, J. Zhang, T. Yamashita, H. Kaji, S. R. Marder, T. Watanabe, C. Adachi, *Adv. Funct. Mater.* **2013**, *23*, 3386.

[9] Z. Yang, L. Mutter, M. Stillhart, B. Ruiz, S. Aravazhi, M. Jazbinsek, A. Schneider, V. Gramlich, P. Günter. *Adv. Funct. Mater.* **2007**, *17*, 2018.

[10] M. S. Wong, C. Bosshard, P. Güter, *Adv. Mater.* **1997**, *9*, 837.

[11] T.-C. Chao, Y.-T. Lin, C.-Y. Yang, T. S. Hung, H.-C. Chou, C.-C. Wu, K.-T. Wong, *Adv. Mater.* **2005**, *17*, 992.

[12] P. N. Prasad, *Introduction to Biophotonics*, Wiley-Interscience, New York **2004**.

[13] K. Watanabe, T. Taniguchi, H. Kanda, *Nat. Mater.* **2004**, *3*, 404.

[14] a) J.-M. Lehn, *Supramolecular Chemistry: Concepts and Perspectives*, VCH, New York **1995**; b) G. R. Desiraju, *Angew. Chem. Int. Ed.* **1995**, *34*, 2311; c) A. Nangia, *Cryst. Growth Des.* **2008**, *8*, 1079; d) G. Cavallo, C. B. Aakeröy, N. R. Champness, C. Janiak, *CrystEngComm* **2010**, *12*, 22; e) T. Friščić, L. R. MacGillivray, *Croat. Chem. Acta.* **2006**, *79*, 327; f) L. R. MacGillivray, G. S. Papaefstathiou, T. Friščić, T. D. Hamilton, K. Bučar, Q. Chu, D. B. Varshney, I. G. Georgiev, *Acc. Chem. Res.* **2008**, *41*, 280.

[15] a) O. Bolton, K. Lee, H. J. Kim, K. Y. Lin, J. Kim, *Nat. Chem.* **2011**, *3*, 205; b) A. Priimagi, G. Cavallo, A. Forni, M. Gorynsztejn–Leben, M. Kaivola, P. Metrangolo, R. Milani, A. Shishido, T. Pilati, G. Resnati, G. Terraneo, *Adv. Funct. Mater.* **2012**, *22*, 2572.

[16] a) J. Kunzelman, M. Kinami, B. R Crenshaw, J. D. Protasiewicz, C. Weder, *Adv. Mater.* **2008**, *20*, 119; b) J. Luo, L.–Y. Li, Y. Song, J. Pei, *Chem. Eur. J.* **2011**, *17*, 10515; c) G. R. Krishna, M. S. R. N. Kiran, C. L. Fraser, U. Ramamurty, C. M. Reddy, *Adv. Funct. Mater.* **2013**, DOI: 10.1002/adfm.201201896.

[17] a) Y. Lei, Q. Liao, H. Fu, J. Yao, *J. Am. Chem. Soc.* **2010**, *132*, 1742; b) O. Braem, T. J. Penfold, A. Cannizzo, M. Chergui, *Phys. Chem. Chem. Phys.* **2012**, *14*, 3513.

[18] T. N. Singh-Rachford, F. N. Castellano, *J. Phys. Chem. A* **2009**, *113*, 5912.

[19] Crystal data for **2A.B**, **2A.C**, **A.D**, **A.E** (CCDC: 926585–926588): can also be obtained free of charge from The Cambridge Crystallographic Data Centre via www.ccdc.cam.ac.uk/data_request/cif.

[20] B. Valeur, *Molecular Fluorescence: Principles and Applications.* Wiley-VCH, Germany **2001**. $r = (I_{VV}–GI_{VH})/(I_{VV}+2GI_{VH})$, where $G = I_{VH}/I_{HH}$, and I_{VH} stands for the photoluminescence intensity obtained with vertical excitation polarized and horizontal detection polarization, and I_{VH}, I_{HV}, I_{HH} are defined in a similar way.

[21] a) T.-Q. Nguyen, J. J. Wu, V. Doan, B. J. Schwartz, S. H. Tolbert, *Science* **2000**, *288*, 652; b) D. P. Yan, J. Lu, M. Wei, J. B. Han, J. Ma, F. Li, D. G. Evans, X. Duan, *Angew. Chem. Int. Ed.* **2009**, *48*, 3073.

[22] a) M. Sase, S. Yamaguchi, Y. Sagara, I. Yoshikawa, T. Mutai, K. Araki, *J. Mater. Chem.* **2011**, *21*, 8347; b) M. Frenette, G. Cosa, T. Friščić, *CrystEngComm* **2013**, *15*, 5100.

[23] For example: a) A. L. Balch, *Angew. Chem. Int. Ed.* **2009**, *48*, 2641; b) Y. Sagara, T. Mutai, I. Yoshikawa, K. Araki, *J. Am. Chem. Soc.* **2007**, *129*, 1520; c) R. Davis, N. P. Rath, S. Das, *Chem. Commun.* **2004**, 74.

[24] For example: a) Y. Sagara, T. Kato, *Angew. Chem. Int. Ed.* **2008**, *47*, 5175; b) Y. Sagara, S. Yamane, T. Mutai, K. Araki, T. Kato, *Adv. Funct. Mater.* **2009**, *19*, 1869; c) V. N. Kozhevnikov, B. Donnio, D. W. Bruce, *Angew. Chem. Int. Ed.* **2008**, *47*, 6286.

[25] For example: a) T. Lasanta, M. E. Olmos, A. Laguna, J. M. López-de-Luzuriaga, P. Naumov, *J. Am. Chem. Soc.* **2011**, *133*, 16358; b) S. H. Lim, M. M. Olmstead, A. L. Balch, *Chem. Sci.* **2013**, *4*, 311.

[26] For example: a) C. Löwe, C. Weder, *Adv. Mater.* **2002**, *14*, 1625; b) S. Srinivasan, P. A. Babu, S. Mahesh, A. Ajayaghosh, *J. Am. Chem. Soc.* **2009**, *131*, 15122; c) J. R. Kumpfer, J. Jin, S. J. Rowan, *J. Mater. Chem.* **2010**, *20*, 145.